Research Article Vol. 2, No. 5 / May 2015 / Optica 405

Energy-dependent photoemission delays from noble metal surfaces by attosecond interferometry

Reto Locher,[1,†] Luca Castiglioni,[2,†,*] Matteo Lucchini,[1] Michael Greif,[2] Lukas Gallmann,[1] Jürg Osterwalder,[2] Matthias Hengsberger,[2] and Ursula Keller[1]

[1]Physics Department, ETH Zurich, CH-8093 Zürich, Switzerland
[2]Department of Physics, University of Zurich, CH-8057 Zürich, Switzerland
*Corresponding author: luca.castiglioni@physik.uzh.ch

Received 8 January 2015; revised 16 March 2015; accepted 24 March 2015 (Doc. ID 232079); published 23 April 2015

How quanta of energy and charge are transported on both atomic spatial and ultrafast timescales is at the heart of modern technology. Recent progress in ultrafast spectroscopy has allowed us to directly study the dynamical response of an electronic system to interaction with an electromagnetic field. Here, we present energy-dependent photoemission delays from the noble metal surfaces Ag(111) and Au(111). An interferometric technique based on attosecond pulse trains is applied simultaneously in a gas phase and a solid-state target to derive surface-specific photoemission delays. Experimental delays on the order of 100 as are in the same time range as those obtained from simulations. The strong variation of measured delays with excitation energy in Ag(111), which cannot be consistently explained invoking solely electron transport or initial state localization as supposed in previous work, indicates that final state effects play a key role in photoemission from solids.

OCIS codes: (260.7120) Ultrafast phenomena; (020.4180) Multiphoton processes; (300.6250) Spectroscopy, condensed matter.

http://dx.doi.org/10.1364/OPTICA.2.000405

1. INTRODUCTION

The dynamical response of the electronic structure of matter to an electromagnetic stimulation, e.g., the absorption of a photon, is responsible for many physical properties as well as the chemical reactivity. Underlying electronic processes naturally occur on an attosecond (1 as $= 10^{-18}$ s) timescale as a result of the characteristic electron velocities and length scales. Photoelectron spectroscopy has been the preeminent tool to study the electronic structure of atoms, molecules, and condensed matter over the past 50 years [1–3]. The energetics of the photoemission process have been understood for a long time [4], but the temporal aspect remained largely unexplored due to the lack of experimental tools with the required attosecond time resolution. The interaction of the outgoing electron with the remaining ion creates a slight delay between photon absorption and electron emission. In the case of photoemission from condensed matter, additional many-body effects such as dynamical screening and electron–electron scattering as well as transport come into play, which further contribute to the photoemission delay. Such subtle effects determine the lineshape in photoelectron spectra [5] or the lifetime of quasiparticles [6] such as plasmons and excitons, which is of fundamental importance for semiconductors and photovoltaic devices [7].

Recent progress in ultrafast spectroscopy [8] has allowed us to directly study the dynamics of electrons in the time domain. Attosecond energy and angular streaking [9,10] and reconstruction of attosecond beating by interference of two-photon transitions (RABBITT) [11,12] are the currently predominant methods to probe ultrafast dynamics on the attosecond timescale. Interaction of the outgoing electron emitted by the attosecond extreme ultraviolet (XUV) pulse with an intense few-cycle infrared (IR) field leads to the formation of sidebands (RABBITT) or changes in the electron momentum (streaking). It has been shown in the atomic case that both RABBITT [11,12] and attosecond streaking [9] deliver the same temporal information about the photoemission process [13]. Whereas streaking was successfully applied to both isolated noble gas atoms and condensed-matter systems, RABBITT has been used exclusively in the gas phase until now to study the photoionization of atoms [14] and molecules [15]. The formation of sidebands (SBs) due to simultaneous absorption of an XUV and an IR photon has been investigated on a platinum surface, but no subcycle dynamics were observed [16].

Attosecond streaking experiments revealed characteristic relative delays between photoelectrons emitted from different electronic states in both noble gas atoms [14,17] and condensed-matter systems [18,19]. Interestingly, different mechanisms were invoked to explain the observed delays. In the atomic case the scattering of the outgoing electron wave packet at the atomic potential leads to a phase shift and thus a delay, as was first proposed by Wigner in 1955 [20]. In condensed matter the situation is more complex as photoemission involves three steps: excitation, transport to the surface, and escape into the vacuum [21]. In the streaking experiments on tungsten [18] and magnesium [19] surfaces it was presumed that streaking of the electron only occurs at the surface or outside the solid, and the observed delays were

explained in terms of transport from the site of initial excitation to the surface. The measured relative delay of 110 as between $4f$ and conduction band electrons in tungsten has been rationalized by various theoretical models. The different emission times were explained in terms of electron transport [22,23], penetration of the surface barrier [24], different initial state localization [23,25], and resonant transitions [26]. A Wigner delay in photoemission from solid surfaces has also been discussed as the consequence of an accumulated phase shift of the propagating wave packet [27] as well as the result of inherent phase shifts associated with final state effects in photoemission [28]. The fact that so many different models were used to reproduce the experimental findings underlines that the dynamics of photoemission in condensed matter are far from being understood and more experimental data are highly needed.

Here, we report a study of energy-dependent photoemission delays from the noble metal surfaces Ag(111) and Au(111). We extended the RABBITT technique to achieve the first observation, to the best of our knowledge, of subcycle dynamics in a condensed-matter system using attosecond pulse trains (APTs). In previous time-resolved photoemission experiments [14,17–19] relative delays between two different initial states of the same physical system were examined. In this work the RABBITT technique is simultaneously applied to argon and to a metal surface. The case of Ar being well understood [13,14,29], it is used to calibrate our setup for the temporal characteristics of the XUV pulse train and its timing relative to the IR pulse. This on-the-fly calibration vastly reduces the susceptibility to experimental instabilities and systematic errors. The simultaneous detection allows us to choose a proper reference to gain access to surface-specific photoemission delays without the need for an intrinsic reference state.

2. SIMULTANEOUS RABBITT MEASUREMENTS IN TWO TARGETS

In order to study photoemission dynamics in solid surfaces the existing attosecond beamline was extended with a surface physics endstation comprising a hemispherical electron analyzer [30]. Figure 1 shows the experimental setup together with typical photon and photoelectron spectra. XUV APTs are produced by high-harmonic generation in argon. Residual IR and low-order harmonic radiation is blocked by a 100 nm Al filter before recombination with the probe beam. A toroidal mirror focuses the copropagating XUV and IR beams into the source of a time-of-flight (ToF) spectrometer where gas phase RABBITT traces are recorded. A second toroidal mirror images the first focus onto a solid sample surface in the source of a hemispherical electron analyzer where RABBITT traces of the metal surfaces are recorded. Both pulses were p polarized, and the angle of incidence on the surface was 75°. Efficient differential pumping kept the pressure in the surface chamber below 7×10^{-10} mbar during the measurements, which allowed us to record RABBITT traces in Ar and on metal surfaces simultaneously. Ag(111) and Au(111) single crystals were cleaned by cycles of sputtering and annealing, and the surface quality was verified by XPS and LEED (details in Section 1 of Supplement 1).

RABBITT offers a temporal resolution comparable to attosecond streaking [9] without the need for a single attosecond pulse with its experimental complexity. The lower intensity requirement of the IR probe field leads to reduced perturbation of the system under study. This renders the method less susceptible to above-threshold photoemission (ATP), which enables access to lower photon energies. In contrast to attosecond streaking, photoemission delays are measured for several photon energies (one per sideband) in one single measurement under the same conditions and for the same initial state. The bandwidth of individual harmonics in the APT of around 1 eV was sufficiently narrow to observe reasonable separation between adjacent replicas in the photoelectron spectra of the investigated surfaces.

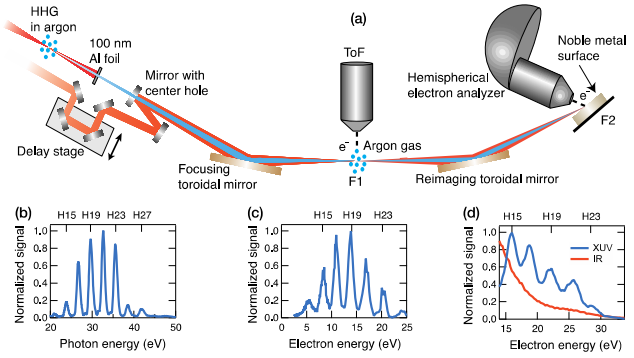

Fig. 1. (a) Schematic illustration of the experiment. (b) Typical photon spectrum of the XUV pulse train. (c) Photoelectron spectrum of Ar. (d) Photoelectron spectra of Ag(111). Replicas of the $4d$ band produced by the harmonics of the XUV pulse sit on a background of secondary electrons (blue line). Moreover, the IR field alone generates an ATP background comparable in strength to the signal of interest (red line).

3. RESULTS

A. Extraction of Surface-Specific Photoemission Phase

A set of experimental RABBITT traces in argon and on Ag(111) is shown in Fig. 2 together with an energy level scheme of the process. In Ar the emitted electrons originate from the $3p$ state; in Ag(111) the $4d$ band is the main contributor. The spectral photoemission phase, $\phi_{2q}^{g/s}$, contains all temporal information and is retrieved by curve fitting [Figs. 2(e) and 2(f)]. The same measurements were repeated for Au(111) with emission from the $5d$ band. Clear differences between the two noble metals were observed (see Fig. 3). The signal background due to secondary electrons and ATP is significantly lower in Au(111) owing to the higher work function of this surface compared to Ag(111).

In general, the work function of a surface is significantly lower than the ionization potential of a noble gas atom. Thus the IR probe field leads to electron emission by ATP at substantially lower intensity. The yield of these electrons strongly decreases with kinetic energy, yet energies of up to 35 eV were observed under experimental conditions [see Fig. 1(d)]. In order to reduce their contribution, relatively low probe intensities were employed (a few times 10^{11} W/cm^2). In addition to ATP, space-charge effects are more severe in a solid-state target due to the high emitter density and obscure the underlying structure of the spectra. Consequently, the flux of the XUV pump pulse was kept low by strongly reducing the intensity of the IR field driving the high-harmonic generation. These specific requirements lead to an unusual intensity regime for RABBITT measurements where the apparent SB amplitude and the depletion of the parent signal appear higher than in previous work [14]. The formalism behind RABBITT to extract photoemission phases from the SB

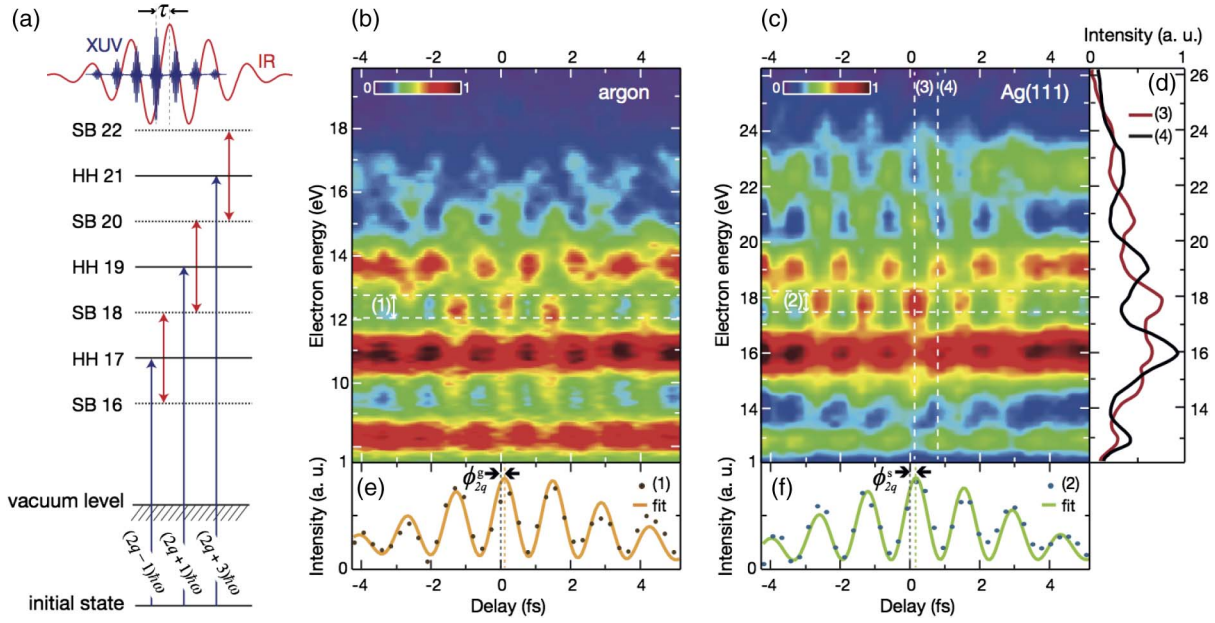

Fig. 2. (a) Energy level scheme of the RABBITT process. Interfering two-color two-photon transitions give rise to sidebands (SBs) between adjacent odd high harmonics (HH). (b),(c) Experimental RABBITT traces from Ar and Ag(111) with electrons originating from Ar $3p$ and Ag $4d$ levels, respectively. Both scans were recorded simultaneously with laser parameters optimized for the surface. A delay-independent background of ATP and secondary electrons was subtracted from (c) to enhance contrast for illustration purposes. (d) Photoelectron spectra from (c) at two different delays. At 100 as (3) the appearance of sidebands is clearly visible, whereas at 800 as (4) the photoelectron spectrum qualitatively resembles the spectrum in the absence of the IR field. (e),(f) Integration over the energy range of SB 18 revealing the oscillation with 2ω. Experimental curves (1) and (2) were fitted with $A(t) \cdot \cos(2\omega t - \phi_{2q})$, where ϕ_{2q} is the experimental spectral phase as indicated and $A(t)$ is the pulse envelope function.

oscillations requires that these sidebands be produced by two-photon transitions (one XUV and one IR photon). Absorption of multiple IR photons can occur at high IR intensities, opening additional quantum paths that may contribute to the oscillating signal and potentially alter the reconstructed photoemission phase [31]. Such higher-order processes would lead to higher frequency contributions of the SB modulation as well as sidebands at harmonic energies exceeding the highest harmonic observed in the XUV spectrum by more than one IR photon. We carefully examined our data but could not find any indication for higher-order processes (see Fig. S1 in Supplement 1). Data sets were taken with varying XUV generation conditions and IR intensities, but retrieved phases remained stable, confirming the surface specificity and robustness of our method.

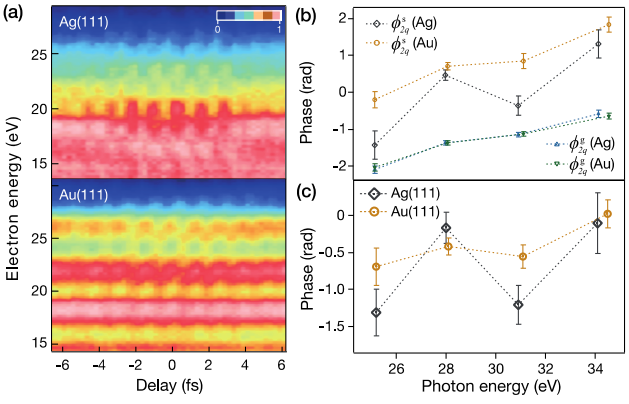

Fig. 3. (a) Raw data of typical RABBITT traces from Ag(111) and Au(111). (b) Raw phases, ϕ_{2q}, extracted from respective surface and argon RABBITT traces. Phases from individual measurements were aligned with the average phase set to zero and contain an unknown offset phase. (c) Surface-specific phase plotted as the phase difference, $\phi^s_{2q} - \phi^g_{2q}$, between corresponding surface and gas phase RABBITT scans. Error bars represent the standard deviation of six scans for Ag(111) and eight scans for Au(111).

B. Derivation of Photoemission Delays

A schematic overview of the RABBITT process for a solid surface is provided in Fig. 4. The Wigner delay, τ^s_λ, (1) due to absorption of a XUV photon and transport within the solid, τ^s_{trans}, (2) contributes to the true photoemission delay. The continuum–continuum interaction with the IR probe field (3) yields an additional measurement-induced delay, τ^s_{cc}. The surface-specific photoemission delays, τ^s_{2q}, for Ag(111) and Au(111) shown in Fig. 5 were obtained as follows:

$$\tau^s_{2q} = \tau^s_{\lambda,2q} + \tau^s_{cc,2q} + \tau^s_{\text{trans},2q} = \frac{\phi^s_{2q} - \phi^g_{2q}}{2\omega} + \tau^g_{\lambda,2q} + \tau^g_{cc,2q} - \tau_{\text{prop}} + \tau_{\text{refl}}. \quad (1)$$

ϕ^g_{2q} and ϕ^s_{2q} are the spectral phases extracted from corresponding surface and gas phase RABBITT traces [see Figs. 2(e) and 2(f) and Figs. 3(b) and 3(c)]. $\tau^g_{\lambda,2q}$ and $\tau^g_{cc,2q}$ characterize our temporal reference, the photoemission in Ar, and are taken from the literature [13,29]. The propagation delay between the two targets, τ_{prop}, arises from a phase shift due to reflection at the toroidal mirror and the Gouy phase difference between the first and second focus. This delay was determined experimentally by performing a simultaneous RABBITT measurement with Ar targets in both foci (see Fig. S2 in Supplement 1). The long focal lengths

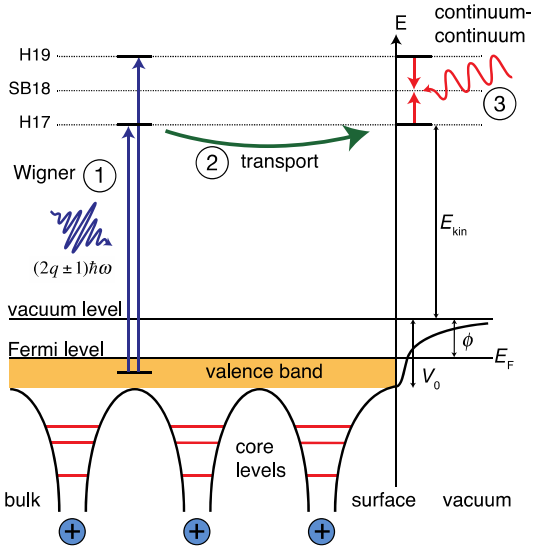

Fig. 4. Schematic representation of the three steps involved in the surface RABBITT: (1) initial excitation of the electron by absorption of an XUV photon, (2) ballistic transport within the solid, and (3) absorption/emission of an IR photon.

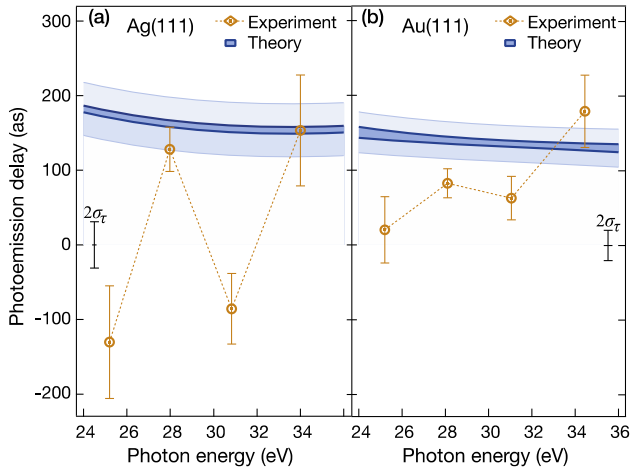

Fig. 5. Experimentally determined photoemission delays. (a) Emission from the Ag(111) 4*d* band (golden diamonds). Results of our simulations are delimited by the extreme cases with and without screening (upper and lower blue lines). (b) Results for emission from the Au(111) 5*d* band. The additional error bars at 0 as in (a) and (b) indicate the experimental error ($2\sigma_\tau$) of the propagation delay, τ_{prop}, which leads to uncertainty in the delay scale. This error is added to the simulated values and illustrated by the light-blue shaded areas for better comparison.

of both toroidal mirrors (1187 mm in F1, 1000 mm in F2) leads to long Rayleigh lengths in F1 and F2 and enables such experimental determination with reasonable precision.

The probe field for the surface measurement consists of the superposition of the incoming IR pulse and the reflected beam, resulting in a transient optical grating. The grazing incidence angle of 15° leads to total reflection, and the solid is only penetrated by a weak evanescent field. Conservation of the electric displacement field leads to a sudden drop of the perpendicular component of the electric field at the vacuum–metal boundary due to the high polarization in these nearly free-electron metals. Accordingly, the intensity of the electric field is nearly two orders of magnitude smaller inside the metal right at the boundary [32–34], and the skin depth on the order of 20 nm that describes the exponential decay of the evanescent wave is unimportant regarding the site of absorption of the IR photon. We can conclude that the interaction of the outgoing photoelectron with the IR field must occur right at the surface since both a strong electric field and a steep potential gradient are only present in its close vicinity. The phase of the effective field was calculated based on Fresnel's equations and taking the specific experimental geometry into account, leading to an additional delay, τ_{refl}.

An alternative model [35] based on optically determined scattering phases [36] was compared to our model. Reflection phases obtained from the two models agree within 0.2 rad, which corresponds to 43 as in our experiment. The phase of the evanescent wave in a gold surface as a function of incidence angle was determined by photon scanning tunneling microscopy and found to be in good agreement with theory based on Fresnel's equations [37]. Furthermore, x-ray optical effects such as total reflection or standing waves at surfaces and inside solids were recently simulated based on Fresnel's equations and also found to reproduce spectroscopy data very well [38].

While the relative delays between photoemission at different energies can be obtained directly from experimental data, in our case, the calibration of the delay scale relies on two model assumptions, i.e., the phase of the effective field at the surface and the description of the temporal reference process [24]. We thus computed the experimental errors for the relative, energy-dependent delays and the absolute timescale separately, since only the zero of the timescale is prone to unknown systematic errors [see Figs. 5(a) and 5(b); details in Section 2 of Supplement 1].

C. Simulation of Photoemission Delays in Solid Surfaces

Our theoretical description employs a composite model based on scattering theory and ballistic transport to simulate photoemission in a solid surface. The Wigner delay due to absorption of the XUV photon and the continuum–continuum delay due to interaction with the IR probe field were calculated based on radial matrix elements and corresponding scattering phase shifts that were computed for dipole-allowed transitions in a muffin-tin potential for Ag and Au [39]. Transport times were derived from a ballistic model with group velocities obtained from fitting free-electron final states to the bulk band structure and taking the inelastic mean-free path (IMFP) at given energies into account. The characteristic timescale of screening was predicted to be around 250 as [40]. Hence, we simulated the limiting cases of an unscreened and a completely screened photohole based on a hydrogen-like potential (see Section 3 of Supplement 1). In our case, the difference is small compared to the overall transport delay due to the small effect of the photohole on the deep potential well in Ag and Au. The monotonic decrease of transport times with increasing kinetic energy is a consequence of both the increasing group velocity and the shape of the universal curve of the IMFP in solids [41]. Contributions from the Wigner delay and τ_{cc}^{s} are smaller and only slightly alter the shape of the computed energy-delay function.

4. DISCUSSION

Calculated and experimental delays in Ag(111) are in good agreement for photon energies of 28 and 34 eV. At other energies, the

experimental delays strongly deviate from the model calculations and are much smaller. A possible explanation for this peculiar result could be that XUV excitation in the probed energy region leads to resonant interband transitions to the Λ_6 *sp* band [42] close to the L_{6+} van Hove singularity with a high density of states. The availability of bulk final states then leads to enhanced emission from the metal bulk, and observed delays are dominated by transport. In the absence of such resonances the photoelectron spectrum is dominated by surface emission [3]. In this regime, electron transport is negligible and observed delays are dominated by τ_λ^s and τ_{cc}^s, resulting in the negative delays observed at 25 and 31 eV. Negative delays were originally predicted by Wigner [20] and also observed in photoemission from Ar atoms [13,14,29]. It must be emphasized that photoemission is treated within the framework of scattering theory and can be considered as a half-collision process. Phase shifts are obtained by comparing the scattered outgoing electron wave to a freely propagating wave with the same wavevector in the asymptotic limit. Hence the temporal reference is the freely propagating wave and not the absorption of the photon. An absolute delay in terms of time elapsed between absorption of a photon and release of the photoelectron is thus not accessible because the exact position of release is not defined in an infinite-range coulombic potential. We estimated the lower limit for the one-photon delay based on Wigner's causality condition [20,43] and obtained a value of −70 as for an electron with 30 eV kinetic energy and a conservative muffin-tin radius of 2 Å.

Delays in Au(111) show less pronounced excursions from the theoretically predicted, transport-dominated behavior. The 5*d* valence band of Au covers a wider energy range than the 4*d* band in Ag, giving rise to additional interband transitions. Bulk emission is therefore more important in Au at these energies, and electron transport cannot be neglected. The interplay between resonant bulk and surface emission has been discussed recently [26] to explain the delays observed in earlier streaking experiments [18,19]. Our experimental data demonstrate that delays in photoemission cannot be solely rationalized by energy-dependent transport times as done in previous studies based on attosecond streaking [18,19]. Conversely, our results suggest that electron transport is only important if bulk final states are available. Both the energetically broad light sources used in the experiment as well as the width of the initial state complicate the observed dynamics. It is likely that both resonant and nonresonant transitions contribute to the measured photoemission phase at each harmonic photon energy. Phase shifts and hence different emission times resulting from resonant transitions were also observed in two-photon ionization experiments of molecular nitrogen [15] and helium [44]. Our model employs spherical harmonics final states and is thus unable to reproduce dynamics induced by resonant transitions. Initial state localization [23,25] has been discussed as a possible origin of different delays observed in the streaking experiments [18,19]. This can be ruled out in our experiment since we probe photoemission from the same initial state at different photon energies. A more sophisticated theoretical treatment of photoemission in solid surfaces is definitely needed but beyond the scope of this work.

5. CONCLUSIONS

The ability to sample energy-dependent and surface-specific photoemission delays affords detailed insight into the ultrafast electron dynamics that goes well beyond the measurement of a plain relative delay. Our experimental data demonstrate that neither electron transport nor initial state localization alone can be invoked to rationalize the measured photoemission delays. The strong energy dependence of the delays indicates that the photoemission dynamics in this energy range are governed by final state effects. We believe that the RABBITT technique will play a major role in the advancement of attosecond science toward condensed-matter systems as it allows for studying charge dynamics at the inherent electronic timescale with less perturbation from the probe process. The higher energy resolution will allow studying the dynamics of such fundamental processes as spin–orbit interaction in systems with sufficiently large spin-orbit splitting. Furthermore, such experiments access the fastest possible response of an electronic system to interaction with an electromagnetic field and hence provide an upper limit for novel electronic devices in the petahertz regime.

NCCR Molecular Ultrafast Science and Technology (NCCR MUST); Swiss National Science Foundation (SNSF); ETH Zurich Postdoctoral Fellowship Program.

We thank P. Krüger for helpful discussions.

†These authors contributed equally to this work.

See Supplement 1 for supporting content.

REFERENCES

1. C. Nordling, E. Sokolowski, and K. Siegbahn, "Precision method for obtaining absolute values of atomic binding energies," Phys. Rev. **105**, 1676–1677 (1957).
2. D. W. Turner and M. I. Al Jobory, "Determination of ionization potentials by photoelectron energy measurement," J. Chem. Phys. **37**, 3007–3008 (1962).
3. S. Hüfner, *Photoelectron Spectroscopy* (Springer, 2003).
4. A. Einstein, "Ueber einen die Erzeugung und Verwandlung des Lichtes betreffenden heuristischen Gesichtspunkt," Ann. Phys.-Berlin **322**, 132–148 (1905).
5. S. Doniach and M. Sunjic, "Many-electron singularity in X-ray photoemission and X-ray line spectra from metals," J. Phys. C **3**, 285 (1970).
6. E. V. Chulkov, I. Sklyadneva, M. Kira, S. W. Koch, J. M. Pitarke, L. M. Sandratskii, P. Buczek, K. Ishioka, J. Schäfer, and M. Weinelt, *Dynamics at Solid State Surfaces and Interfaces*, Vol. **2**: Fundamentals (Wiley-VCH, 2012).
7. S. M. Sze, *Physics of Semiconductor Devices* (Wiley, 2007).
8. M. Hentschel, R. Kienberger, C. Spielmann, G. A. Reider, N. Milosevic, T. Brabec, P. Corkum, U. Heinzmann, M. Drescher, and F. Krausz, "Attosecond metrology," Nature **414**, 509–513 (2001).
9. J. Itatani, F. Quéré, G. L. Yudin, M. Y. Ivanov, F. Krausz, and P. B. Corkum, "Attosecond streak camera," Phys. Rev. Lett. **88**, 173903 (2002).
10. P. Eckle, A. N. Pfeiffer, C. Cirelli, A. Staudte, R. Dörner, H. G. Muller, M. Büttiker, and U. Keller, "Attosecond ionization and tunneling delay time measurements in helium," Science **322**, 1525–1529 (2008).
11. P. M. Paul, E. S. Toma, P. Breger, G. Mullot, F. Augé, P. Balcou, H. G. Muller, and P. Agostini, "Observation of a train of attosecond pulses from high harmonic generation," Science **292**, 1689–1692 (2001).
12. H. G. Muller, "Reconstruction of attosecond harmonic beating by interference of two-photon transitions," Appl. Phys. B **74**, S17–S21 (2002).
13. J. M. Dahlström, D. Guénot, K. Klünder, M. Gisselbrecht, J. Mauritsson, A. L'Huillier, A. Maquet, and R. Taïeb, "Theory of attosecond delays in laser-assisted photoionization," Chem. Phys. **414**, 53–64 (2013).
14. K. Klünder, J. M. Dahlström, M. Gisselbrecht, T. Fordell, M. Swoboda, D. Guenot, P. Johnsson, J. Caillat, J. Mauritsson, A. Maquet, R. Taïeb, and A. L'Huillier, "Probing single-photon ionization on the attosecond time scale," Phys. Rev. Lett. **106**, 143002 (2011).

15. S. Haessler, B. Fabre, J. Higuet, J. Caillat, T. Ruchon, P. Breger, B. Carre, E. Constant, A. Maquet, E. Mevel, P. Salieres, R. Taieb, and Y. Mairesse, "Phase-resolved attosecond near-threshold photoionization of molecular nitrogen," Phys. Rev. A **80**, 011404 (2009).
16. L. Miaja-Avila, C. Lei, M. Aeschlimann, J. L. Gland, M. M. Murnane, H. C. Kapteyn, and G. Saathoff, "Laser-assisted photoelectric effect from surfaces," Phys. Rev. Lett. **97**, 113604 (2006).
17. M. Schultze, M. Fiess, N. Karpowicz, J. Gagnon, M. Korbman, M. Hofstetter, S. Neppl, A. L. Cavalieri, Y. Komninos, T. Mercouris, C. A. Nicolaides, R. Pazourek, S. Nagele, J. Feist, J. Burgdorfer, A. M. Azzeer, R. Ernstorfer, R. Kienberger, U. Kleineberg, E. Goulielmakis, F. Krausz, and V. S. Yakovlev, "Delay in photoemission," Science **328**, 1658–1662 (2010).
18. A. L. Cavalieri, N. Müller, T. Uphues, V. S. Yakovlev, A. Baltuska, B. Horvath, B. Schmidt, L. Blümel, R. Holzwarth, S. Hendel, M. Drescher, U. Kleineberg, P. M. Echenique, R. Kienberger, F. Krausz, and U. Heinzmann, "Attosecond spectroscopy in condensed matter," Nature **449**, 1029–1032 (2007).
19. S. Neppl, R. Ernstorfer, E. M. Bothschafter, A. L. Cavalieri, D. Menzel, J. V. Barth, F. Krausz, R. Kienberger, and P. Feulner, "Attosecond time-resolved photoemission from core and valence states in magnesium," Phys. Rev. Lett. **109**, 087401 (2012).
20. E. P. Wigner, "Lower limit for the energy derivative of the scattering phase shift," Phys. Rev. **98**, 145 (1955).
21. C. N. Berglund and W. E. Spicer, "Photoemission studies of copper and silver: theory," Phys. Rev. **136**, A1030–A1044 (1964).
22. C. Lemell, B. Solleder, K. Tökesi, and J. Burgdörfer, "Simulation of attosecond streaking of electrons emitted from a tungsten surface," Phys. Rev. A **79**, 062901 (2009).
23. C.-H. Zhang and U. Thumm, "Attosecond photoelectron spectroscopy of metal surfaces," Phys. Rev. Lett. **102**, 123601 (2009).
24. J. C. Baggesen and L. B. Madsen, "Theory for time-resolved measurements of laser-induced electron emission from metal surfaces," Phys. Rev. A **78**, 032903 (2008).
25. A. K. Kazansky and P. M. Echenique, "One-electron model for the electronic response of metal surfaces to subfemtosecond photoexcitation," Phys. Rev. Lett. **102**, 177401 (2009).
26. A. G. Borisov, D. Sanchez-Portal, A. K. Kazansky, and P. M. Echenique, "Resonant and nonresonant processes in attosecond streaking from metals," Phys. Rev. B **87**, 121110 (2013).
27. C.-H. Zhang and U. Thumm, "Streaking and Wigner time delays in photoemission from atoms and surfaces," Phys. Rev. A **84**, 033401 (2011).
28. U. Heinzmann and J. H. Dil, "Spin–orbit-induced photoelectron spin polarization in angle-resolved photoemission from both atomic and condensed matter targets," J. Phys. Condens. Matter **24**, 173001 (2012).
29. J. Mauritsson, M. B. Gaarde, and K. J. Schafer, "Accessing properties of electron wave packets generated by attosecond pulse trains through time-dependent calculations," Phys. Rev. A **72**, 013401 (2005).
30. R. Locher, M. Lucchini, J. Herrmann, M. Sabbar, M. Weger, A. Ludwig, L. Castiglioni, M. Greif, M. Hengsberger, L. Gallmann, and U. Keller, "Versatile attosecond beamline in a two-foci configuration for simultaneous time-resolved measurements," Rev. Sci. Instrum. **85**, 013113 (2014).
31. M. Swoboda, J. M. Dahlström, T. Ruchon, P. Johnsson, J. Mauritsson, A. L'Huillier, and K. J. Schafer, "Intensity dependence of laser-assisted attosecond photoionization spectra," Laser Phys. **19**, 1591–1599 (2009).
32. A. T. Georges, "Calculation of surface electromagnetic fields in laser–metal surface interaction," Opt. Commun. **188**, 321–331 (2001).
33. K. L. Kliewer, "Electromagnetic effects at metal surfaces: a nonlocal view," Surf. Sci. **101**, 57–83 (1980).
34. E. E. Krasovskii, V. M. Silkin, V. U. Nazarov, P. M. Echenique, and E. V. Chulkov, "Dielectric screening and band-structure effects in low-energy photoemission," Phys. Rev. B **82**, 125102 (2010).
35. U. Bovensiepen, S. Declair, M. Lisowski, P. A. Loukakos, A. Hotzel, M. Richter, A. Knorr, and M. Wolf, "Ultrafast electron dynamics in metals: real-time analysis of a reflected light field using photoelectrons," Phys. Rev. B **79**, 045415 (2009).
36. P. B. Johnson and R. W. Christy, "Optical constants of the noble metals," Phys. Rev. B **6**, 4370 (1972).
37. J. Jose, F. B. Segerink, J. P. Korterik, and H. L. Offerhaus, "Near-field observation of spatial phase shifts associated with Goos–Haenschen and surface plasmon resonance effects," Opt. Express **16**, 1958–1964 (2008).
38. S.-H. Yang, A. X. Gray, A. M. Kaiser, B. S. Mun, and B. C. Sell, "Making use of x-ray optical effects in photoelectron-, Auger electron-, and x-ray emission spectroscopies: total reflection, standing-wave excitation, and resonant effects," J. Appl. Phys. **113**, 073513 (2013).
39. O. K. Andersen, Z. Pawlowska, and O. Jepsen, "Illustration of the linear-muffin-tin-orbital tight-binding representation: compact orbitals and charge density in Si," Phys. Rev. B **34**, 5253–5269 (1986).
40. R. D. Muiño, D. Sánchez-Portal, V. M. Silkin, E. V. Chulkov, and P. M. Echenique, "Time-dependent electron phenomena at surfaces," Proc. Natl. Acad. Sci. U.S.A. **108**, 971–976 (2011).
41. A. Zangwill, *Physics at Surfaces* (Cambridge University, 1988).
42. H. Eckardt, L. Fritsche, and J. Noffke, "Self-consistent relativistic band structure of the noble metals," J. Phys. F **14**, 97 (1984).
43. C. A. A. d. Carvalho and H. M. Nussenzveig, "Time delay," Phys. Rep. **364**, 83–174 (2002).
44. M. Swoboda, T. Fordell, K. Klünder, J. M. Dahlström, M. Miranda, C. Buth, K. J. Schafer, J. Mauritsson, A. L'Huillier, and M. Gisselbrecht, "Phase measurement of resonant two-photon ionization in helium," Phys. Rev. Lett. **104**, 103003 (2010).